



Study on a novel PTFE membrane with regular geometric pore structures fabricated by near-field electrospinning, and its applications

Jinxue Cheng^a, Qinglin Huang^{a,*}, Yan Huang^a, Wei Luo^a, Quan Hu^b, Changfa Xiao^a

^a State Key Laboratory of Separation Membranes and Membrane Processes/ National Center for International Joint Research on Separation Membranes, Department of Material Science and Engineering, Tiangong University, Tianjin, 300387, PR China

^b Changsha Nanoapparatus Co., Ltd, Changsha, 410017, PR China



ARTICLE INFO

Keywords:

Poly(tetrafluoroethylene) (PTFE)
Near-field electrospinning (NFES)
Pore geometry
Oil/water separation
Particle sequential separation

ABSTRACT

Novel poly(tetrafluoroethylene) (PTFE) membranes with regular geometric pore structure were fabricated via near-field electrospinning (NFES) method.

Firstly, computer aided design (CAD) was utilized to design membrane's pore geometry (triangle, diamond, square, hexagon and their different size). Secondly, the PTFE spinning solution consisted of PTFE emulsion and carrier (PVA aqueous solution) was electrospun into nascent PTFE/PVA membrane, which had regular geometric pore structure. Finally, the nascent membrane suffered sintering process, and the NFES PTFE membrane was obtained. Effects of PTFE/PVA mass ratio, sintering temperature and annealing condition, pore geometry on the membrane morphology, structure and properties were investigated, respectively. Results found that the square membrane showed good combination of membrane performances and properties, when PTFE/PVA mass ratio was 6:1 and sintered at 380 °C followed by cooling in muffle furnace. Owing to the excellent hydrophobicity, the obtained PTFE membranes exhibited excellent oil/water separation performance in terms of high oil flux (707 L m⁻² h⁻¹) without extra pressure, and high separation efficiency (rejection up to 99.6%). Owing to the regular and accurate pore structure, the PTFE membrane was utilized in the particle sequential separation. The mixed silica (SiO₂) particles with a series of diameter (1, 5, 10, 20 μm) were sequential separated by PTFE membranes with different pore geometry, and the rejection reached up to 82.0%.

1. Introduction

In recent years, membrane separation technology has been widely explored due to its irreplaceable advantages, such as environmental friendly, low energy consumption, high separation efficiency, flexibility and space saving, and so on [1–6]. Polytetrafluoroethylene (PTFE) is well known for its outstanding chemical resistance, thermal stability, low surface friction, strong hydrophobicity, and self-cleaning performances [7–12], which makes it an ideal membrane materials for membrane application, such as industrial filter, membrane contactor (MC) and so on. However, the high melt viscosity (about 10 G Pa s) [13] and dissolving difficultly in most of organic solvents make it a major challenge for PTFE membranes fabrication by phase inversion process or melt-spinning methods [14]. Generally speaking, PTFE flat-sheet membranes with node-fiber pore geometry are predominantly fabricated by biaxial stretching method [15]. However, the disadvantages of biaxial stretching are the difficult controllability of membrane pore size

and pore geometry. Paste extrusion method is usually used to prepare PTFE hollow fiber membrane. Zhu et al. [16] prepared PTFE hollow fiber membranes through paste extrusion, stretching and sintering process. However, this method is complicated and considered to be environmentally unfriendly, because it requires a certain amount of lubricant when the paste was extruded [17].

Near-field electrospinning (NFES) has attracted the attention as a novel technique to fabricate nanomaterials by superposing layer-by-layer of polymers on a planer substrate under the action of an electric field [18]. Compared with conventional electrospinning technology, NFES has the advantages of a shorter spinning distance, lower supply voltage, more complex structure and controlled deposition [19]. NFES technology can restrict the phenomenon of fiber bending during electrospinning due to the lower spinning distance. Meanwhile, NFES technology don't need any complicated post-treatment process, which would reduce the production cost. Middleton et al. [20] prepared the PCL and PCL/collagen fiber membranes by NFES, and an interconnected

* Corresponding author. Tiangong University, 399 West Binshui Road, Xiqing District, 300387, Tianjin, PR China.
E-mail address: huangqinglin@tjpu.edu.cn (Q. Huang).

Table 1

The code and composition of the spinning solution.

Code	PTFE/PVA (wt/wt)	Sintered membranes code
1	4:1	M-4
2	6:1	M-6
3	8:1	M-8
4	10:1	M-10

fiber networks were obtained by adjusting the spinning parameters. Bisht et al. [21] verified the nanofiber with continuous patterns can be obtained by NFES technology.

In our previous work, we fabricated ultrafine fibrous PTFE hollow fiber membranes through electrospinning technology, and the obtained membranes showed outstanding performances of hydrophobicity, thermal resistance [22]. The main objective of this study is providing a novel method of fabricating PTFE membrane with regular geometric pore structure by NFES. We explored the effects of PTFE/PVA mass ratio, sintering condition and pore geometry on NFES PTFE membrane's pore structure and properties.

2. Experimental

2.1. Materials

Poly (vinyl alcohol) (PVA, Type 1788) was purchased from Aladdin Industrial Co., Ltd, Shanghai, China. PTFE emulsion was purchased from

3F New Materials Co., Ltd, Shanghai, China. Boric acid was purchased from Ying da Rare Chemical Reagents Factory, Tianjin, China. The more characteristics can be found in our previous work [15]. Kerosene, diesel oil, vegetable oil, trichloromethane and vacuum pump oil supplied by Tianjin Kailida Chemical Co., Ltd, Tianjin, China. Sudan III and methylene blue were purchased from Shanghai Macklin Biochemical Co., Ltd, China. SiO_2 with a series of particle size were obtained from Shanghai Pantian Nano Materials Co., Ltd, Shanghai, China.

2.2. Membrane fabrication

A homogeneous PTFE/PVA spinning solution was prepared by mixing 10 wt% PVA aqueous solution, PTFE emulsion and a certain amount of boric acid for 6 h at room temperature. The composition of the spinning solution was tabulated in Table 1.

Fig. 1 showed the preparation process of NFES PTFE membrane. The NFES equipment was mainly divided into four parts: computer programming device, pressurized feeding device, electricity power supply device and direct writing device. Computer programming device was used to design membrane's pore geometry such as triangle, diamond, square and hexagon. Pressurized feeding device and the power supply device was used to inject the spinning solution into the direct writing device. Firstly, the spinning solution was electrospun into nascent PTFE/PVA membranes with the spinning parameters shown in Table 2. Secondly, the nascent membranes were sintered in a muffle furnace in air atmosphere at 380 °C for 5 h (heating rate 1 °C/min). Finally, the NFES PTFE membranes were obtained, and the parameters and codes were

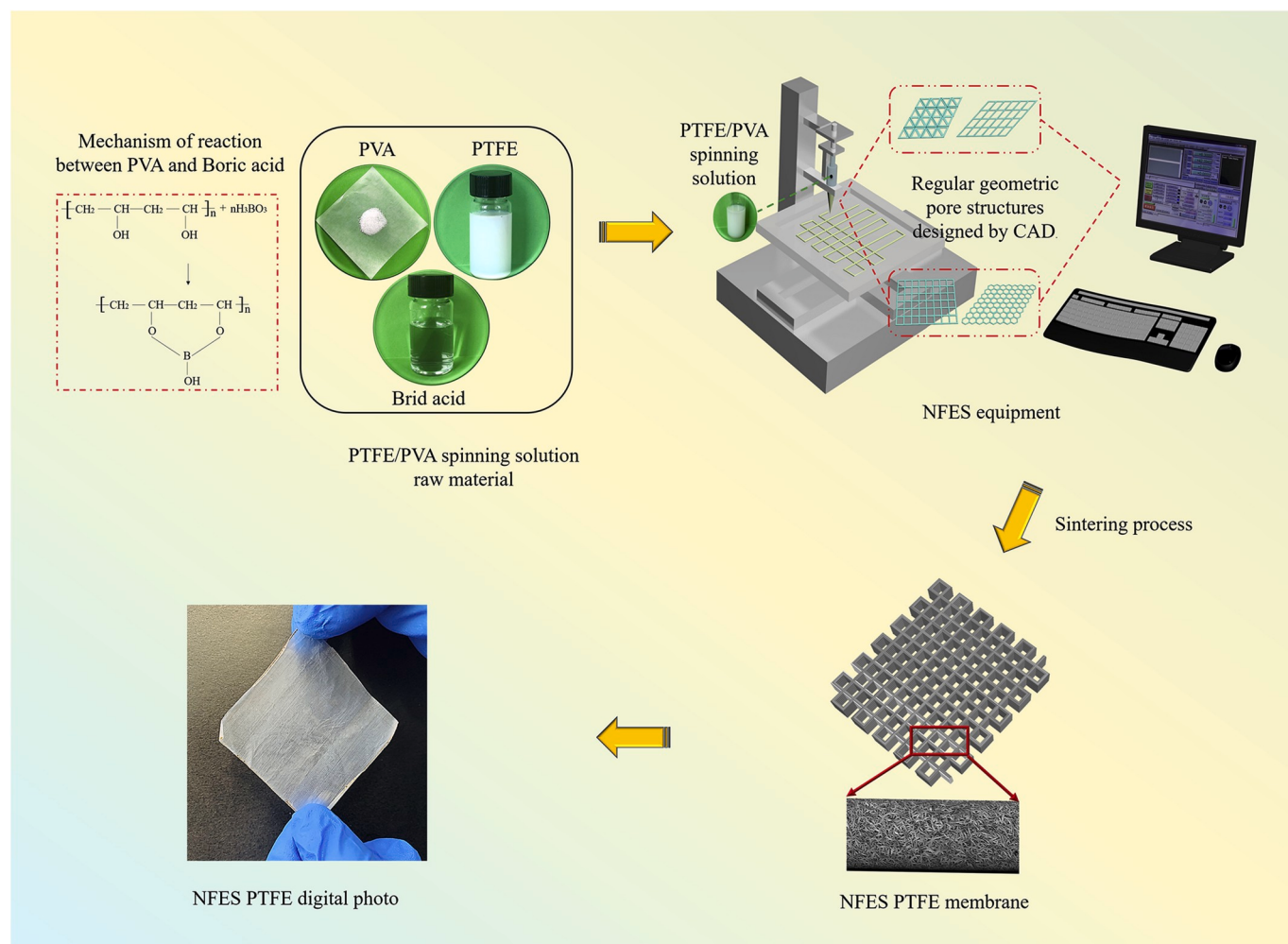


Fig. 1. Schematic diagram of PTFE membrane fabrication by NFES.

Table 2

The parameters of electrospinning nascent PTFE/PVA membranes.

Characteristic	Value
Spinneret/collector distance (cm)	4
Applied voltage (kV)	2.85
Fluid flow rate ($\mu\text{L}/\text{min}$)	4.2
Temperature ($^{\circ}\text{C}$)	25 \pm 5
Relative humidity (%)	40 \pm 10
Printing layer	6

Table 3

The parameters and codes of the sintered PTFE membranes.

Code	Side length (mm)	Printing layer	Pore geometry	Sintered membranes code
1	0.2	6	Triangular	M-S1
2	0.2	6	Diamond	M-S2
3	0.2	6	Square	M-S3
4	0.2	6	Hexagonal	M-S4

tabulated in Table 3.

2.3. Membrane characterization

2.3.1. Rheological characterization

The rheological properties of PTFE/PVA spinning solution were characterized using a HAAKE rotational rheometer (HAAKE MARS, Thermo Fisher Scientific) with a thermostatic bath at a temperature of 25 °C. The relationship between the viscosity and shear rate was obtained at a shear rate range of 0–1000 s⁻¹.

2.3.2. Membrane morphologies

The NFES PTFE membrane morphologies were evaluated by scanning electron microscopy (FESEM, S4800, Japan; SEM TM3030, Japan) and optical microscope after coating the membranes with gold. The membranes' surface roughness was observed by confocal laser scanning microscope (CLSM, Zeiss CSM700, Germany).

2.3.3. Thermogravimetric analysis (TGA)

The thermal degradation behavior of the NFES PTFE membrane was monitored by using a thermogravimetric analysis instrument (TG, TG 209 F3 Tarsus, Germany) under air atmosphere from 25 °C to 800 °C at a heating rate of 5 °C/min.

2.3.4. Fourier transform infrared (FTIR)

Membrane's surface chemistry composition was verified by Fourier-transform infrared spectroscopy (FTIR, Nicolet iS5, iD7 ATR, USA) in the range of 4000–500 cm⁻¹ under a transmittance mode.

2.3.5. Hydrophobicity and lipophilicity

Membrane's hydrophobicity and lipophilicity were measured through static water contact angle and oil contact angle by an optical contact angle meter (model DSA100, Germany) with a 0.3 μL droplet at room temperature by the sessile drop method. The average value of ten different spots were recorded for each sample.

2.3.6. Thermal and crystalline behavior

Thermal behavior of NFES PTFE membranes with different sintering temperatures and cooling rates were analyzed using different scanning calorimeter measurements (DSC, 204F1, Germany) under an operated temperature range from 25 °C to 400 °C at a rate of 10 °C/min. The degrees of crystallization were calculated according to

$$X_C = \frac{\Delta H}{\Delta H_f} \times 100\% \quad (1)$$

where ΔH is the enthalpy of fusion of the membrane (J/g) and the ΔH_f is the enthalpy of fusion for 100% crystalline of PTFE membrane (80J/g) [23].

The crystalline phases of the NFES PTFE membranes were investigated by X-ray diffraction measurements (XRD, D8 DISCOVER, Bruker, Karlsruhe, Germany).

2.3.7. Oil/water separation performance

The oil/water mixture (1:1, v/v) separation performance was measured by Fig. 2. The oil/water mixture was composed of kerosene dyed by Sudan III while distilled water dyed by methylene blue. The oil/water mixture was poured into the tilted solvent filter. No extra pressure was employed during the separation process. Oil/water separation efficiency was calculated according to

$$\eta = \frac{V_1 - V_2}{V_3} \times 100\% \quad (2)$$

where η is the oil/water separation efficiency (%), V_1 is the volume of collected oil after separation (mL), V_2 is the volume of collected water after separation (mL), V_3 is the volume of oil before separation (mL). The permeation flux was calculated by

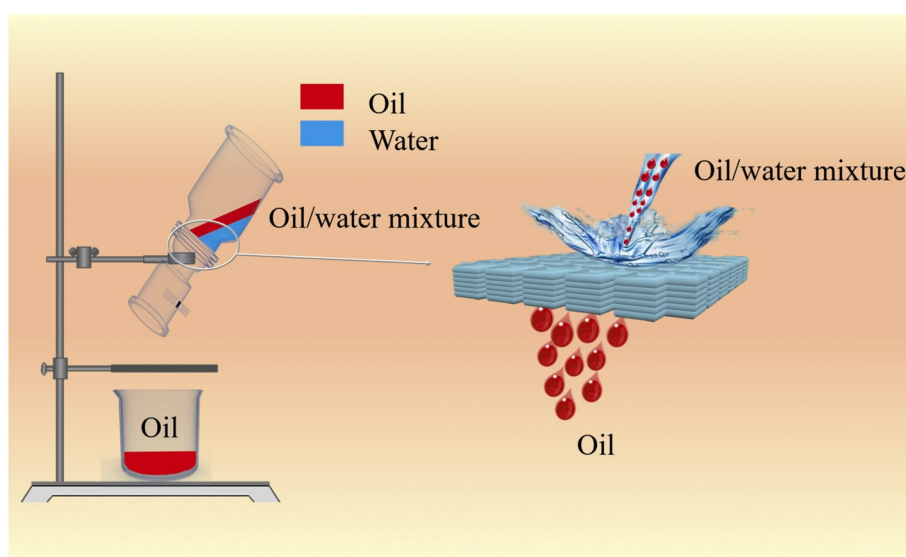


Fig. 2. Schematic diagram of oil/water separation test.

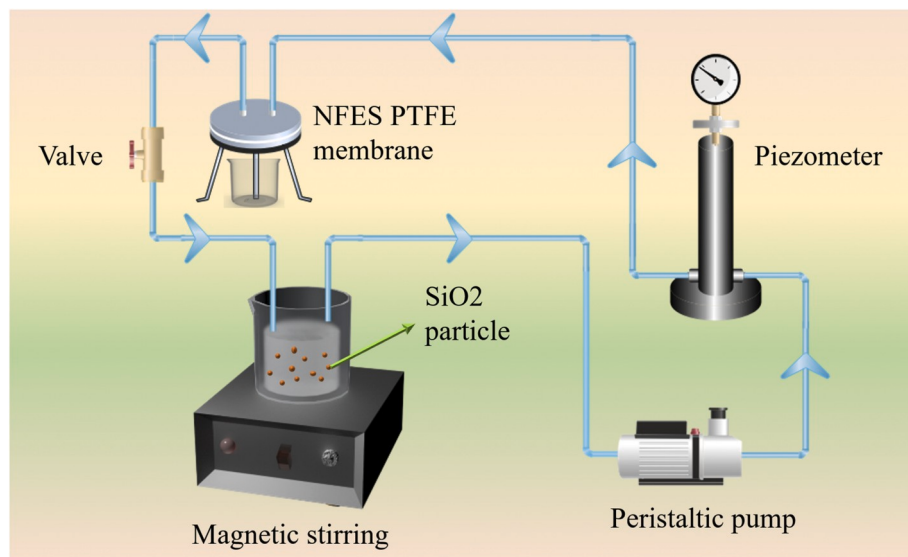


Fig. 3. Schematic diagram of particle filtration test.

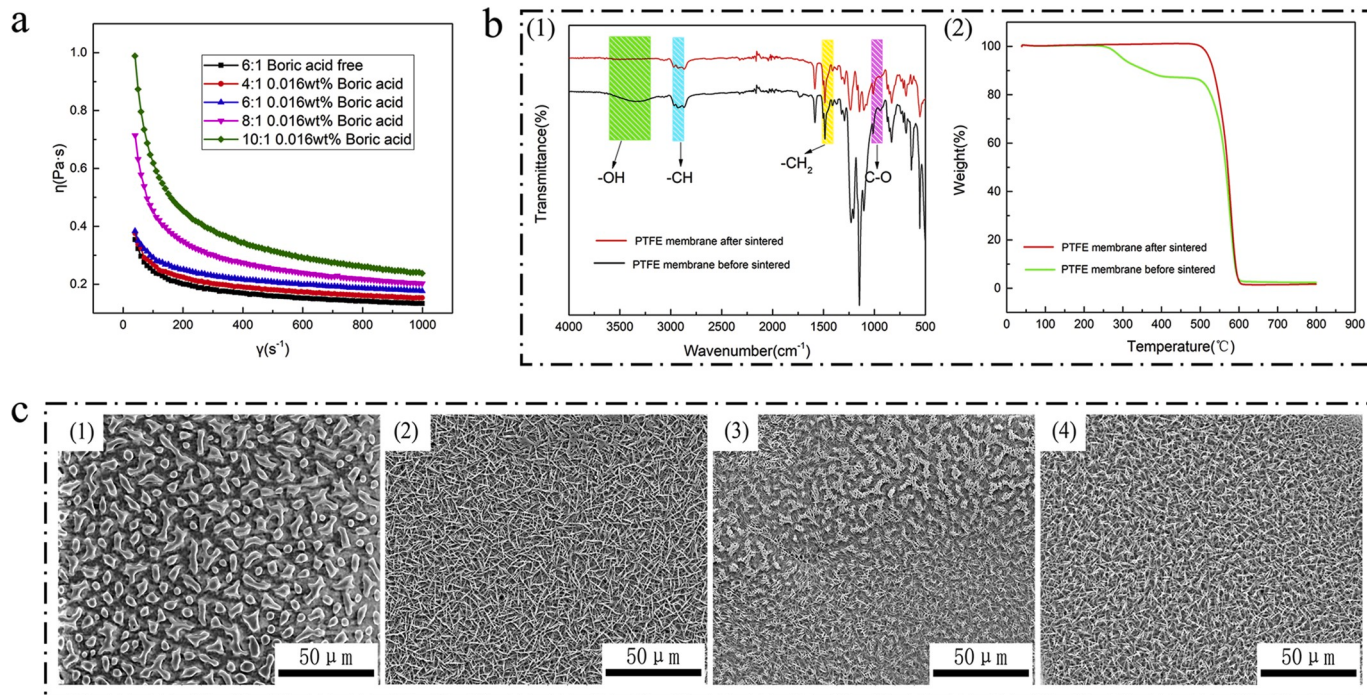


Fig. 4. (a) Rheological behavior of various PTFE/PVA spinning solution; (b) Composition comparison of PTFE membrane before and after sintering: (1) FTIR spectra, (2) TG curves; (c) SEM images of membranes with different mass ratio: (1) M-4, (2) M-6, (3) M-8, (4) M-10.

$$J = \frac{V}{A \times T} \quad (3)$$

where J is the oil flux ($\text{L}\cdot\text{m}^{-2}\cdot\text{h}^{-1}$), V is the total volume of the collected oil (L), A is the effective membrane area (m^2), T is the operation time (h).

In order to characterize the reuse performance of the NFES PTFE membranes, the oil flux recovery was carried out. The membrane was taken out after running for 5 min, and then was rinsed with alcohol for 1 min. Finally, the membrane was utilized in next round of oil-water separation experiment. The experiments were repeated for 10 times, and the flux recovery rate was calculated as follows:

$$FR = \frac{J_1}{J_0} \times 100\% \quad (4)$$

where FR is the flux recovery rate (%), J_1 is the flux after cleaning ($\text{L}\cdot\text{m}^{-2}\cdot\text{h}^{-1}$), J_0 is the original flux ($\text{L}\cdot\text{m}^{-2}\cdot\text{h}^{-1}$).

2.3.8. SiO_2 particle sequential separation

The particle sequential separation was tested using SiO_2 with a series of particle sizes (20 μm , 10 μm , 5 μm and 1 μm), which were dispersed in distilled water (SiO_2 concentration 0.1 wt%). The NFES PTFE membranes with different pore geometry were used for particle filtration test, the schematic of particle filtration was shown in Fig. 3. The flux calculation was as shown in Eq. (3), the feed solution and permeate water was subjected to UV-spectrophotometry and the rejection rate R was calculated by Eq. (5):

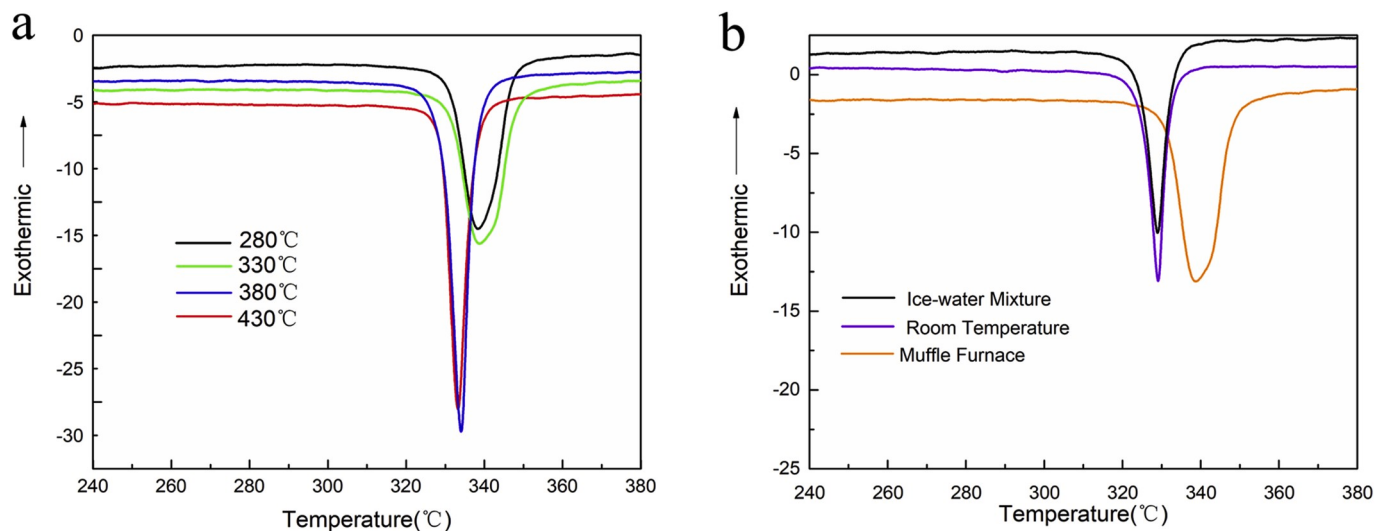


Fig. 5. Membrane's DSC curves: (a) different sintering temperatures; (b) different anneal temperatures.

Table 4

Effect of sintering temperature and annealing conditions on melting point and crystallinity of PTFE membrane.

	Sintering temperature (°C)				Annealing condition		
	280	330	380	430	Ice-water Mixture	Indoor Temperature	Muffle Furnace
Melting point (°C)	338	338	334	333	329	329	339
Crystallinity (%)	91.0	93.9	97.1	93.9	38.0	41.5	97.1

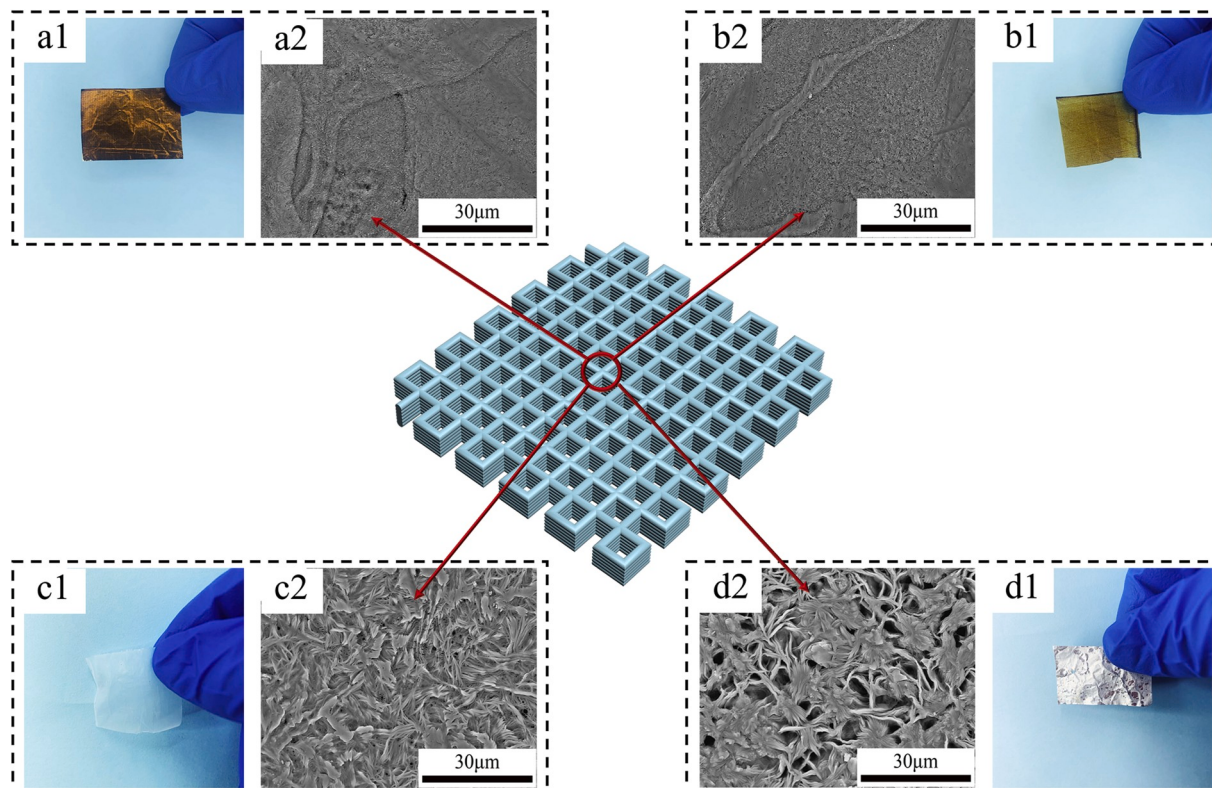


Fig. 6. The (1) digital images and (2) SEM images of M-S3 at different sintering temperature: (a) 280 °C; (b) 330 °C; (c) 380 °C; (d) 430 °C.

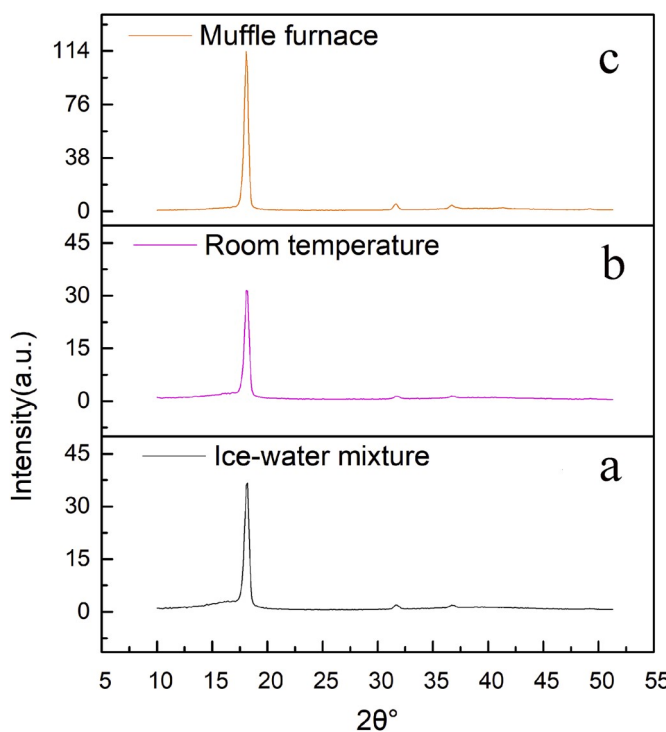


Fig. 7. XRD patterns with different annealing conditions.

$$R = \left(1 - \frac{C_2}{C_1}\right) \times 100\% \quad (5)$$

where C_1 and C_2 are the concentration of the feed solution and permeate water, respectively.

3. Results and discussion

3.1. Membrane morphology and structure

3.1.1. Effects of PTFE/PVA mass ratio

The rheological behaviors of PTFE/PVA spinning solution were shown in Fig. 4a. It can be seen that the viscosity of the spinning solution decreased gradually with the increase of shear rate and the PTFE/PVA mass ratio. The addition of PTFE particles led to a significant increase in the viscosity of the PTFE/PVA spinning solution which made the spinning solution exhibit a behavior of non-Newtonian fluid. Meanwhile, the FTIR and TG results shown in Fig. 4b demonstrated that there only PTFE left while PVA decomposed after sintering process. Fig. 4c showed the changes of sintered NFES PTFE membranes' surface morphology with various PTFE/PVA mass ratios. When the PTFE/PVA mass ratio increased from 4:1 to 10:1, NFES PTFE membrane's surface morphology changed significantly. When the PTFE/PVA mass ratio was 4:1, there were enough free volume among PTFE resin after the decomposition of PVA by sintering process. Therefore, PTFE would form a relatively complete crystals which showed the micro aggregates in Fig. 4(c1) [24]. When the PTFE/PVA mass ratio increased, the free volume of PTFE was compressed which limited the growth of PTFE crystal, and showed smaller size of the micro aggregates in Fig. 4(c4). When the PTFE/PVA mass ratio was 6:1, NFES PTFE membranes' surface exhibited fibrous structures, and they were evenly distributed. So we chose the PTFE/PVA mass ratio 6:1 for the spinning solution.

3.1.2. Effects of sintering temperature and annealing condition

Fig. 5 showed the effects of sintering temperature and annealing conditions on the crystallinity of NFES PTFE membranes. Results of

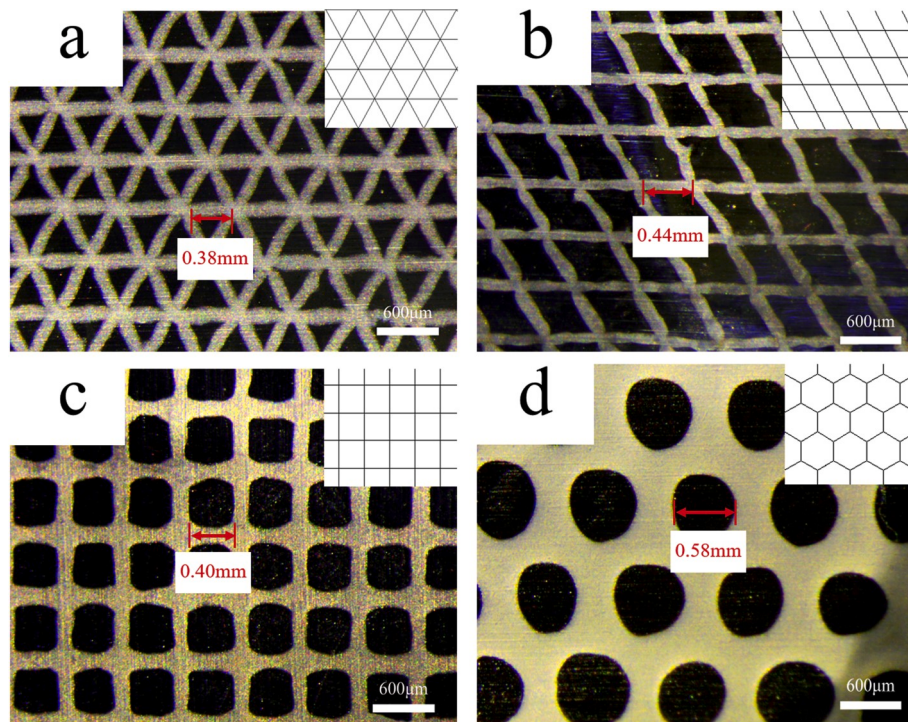


Fig. 8. Optical microscope images of monolayer NEFS PTFE membrane with different pore geometry: (a) triangle; (b) diamond; (c) square; (d) hexagon. Insets were the photos of CAD design with side length of 0.6 mm.

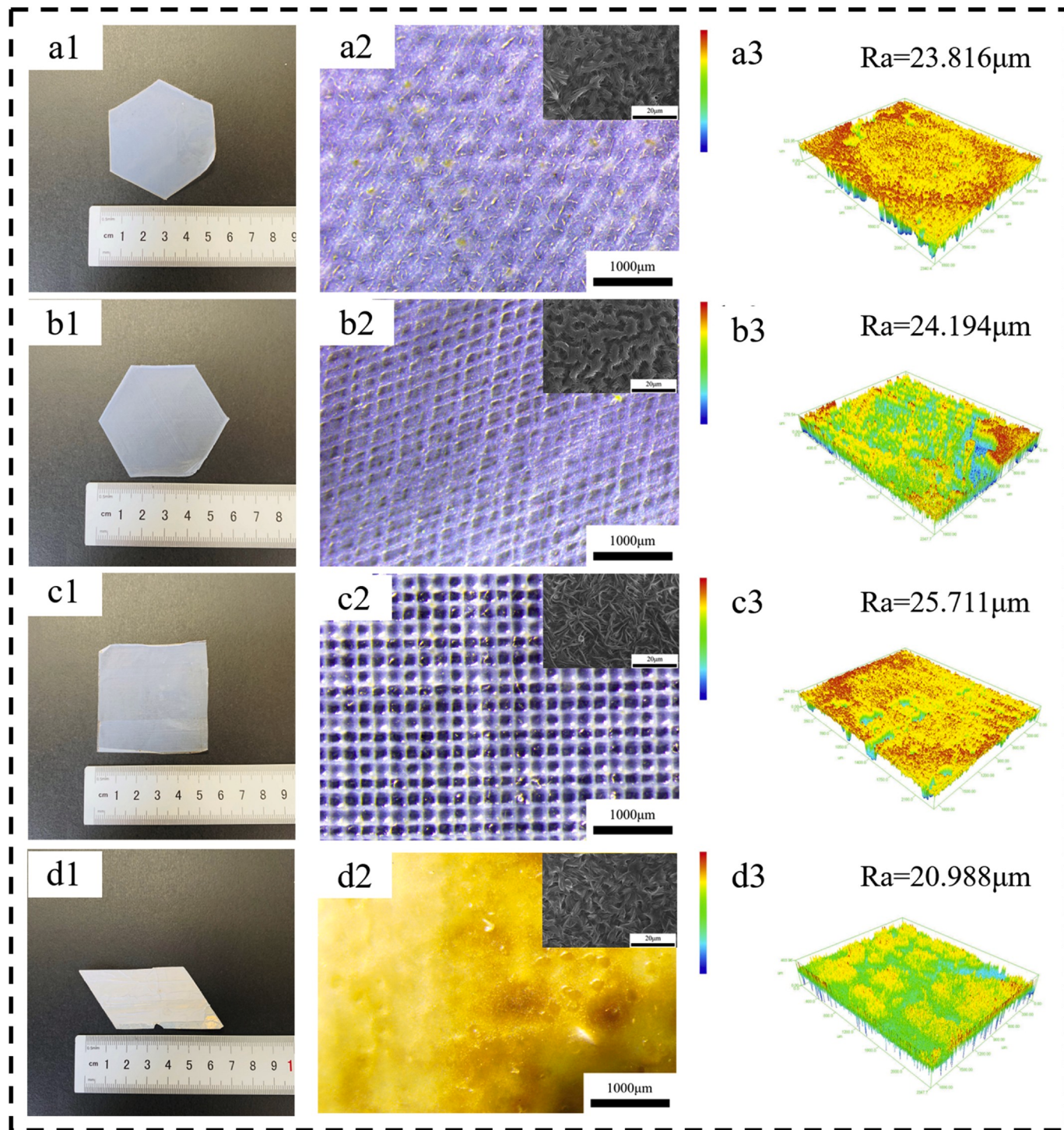


Fig. 9. The (1) digital images, (2) optical microscope images ($\times 13.2$) and (3) 3D CLSM images of NFES PTFE membrane: (a) M-S1; (b) M-S2; (c) M-S3; (d) M-S4.

membrane's melting point and crystallinity were shown in Table 4.

The morphologies of M-S3 membranes (sintering at 280 °C, 330 °C, 380 °C and 430 °C) were shown in Fig. 6. It can be found that the membrane color became lighter and the particular fibrous structure of PTFE appeared with the increase of sintering temperature. As the temperature rose to 380 °C, the PVA decomposed completely and the membrane color became milky white, during which the membrane had the highest crystallinity of 97.1% (Table 4). However, there was defects on the membrane's surface owing to the heat shrinkage when the sintering temperature exceeded 380 °C.

The crystallinity of NFES PTFE membranes with different annealing

conditions were shown in Fig. 7. It can be seen that the diffraction peaks were generated at $2\theta = 18^\circ$, which corresponded to the diffraction of the (100) plane in semi-crystalline PTFE. In Fig. 7c, the XRD curves showed the sharpest diffraction peaks, which demonstrated the highest crystallization of NFES PTFE membrane after cooling in muffle furnace, and it was consistent with the DSC results. From the above analysis, we chose the optimum sintering condition: sintering temperature of 380 °C, and annealing condition of cooling in the muffle furnace.

3.1.3. Effects of pore geometry

Fig. 8 showed the optical microscope images of monolayer NFES

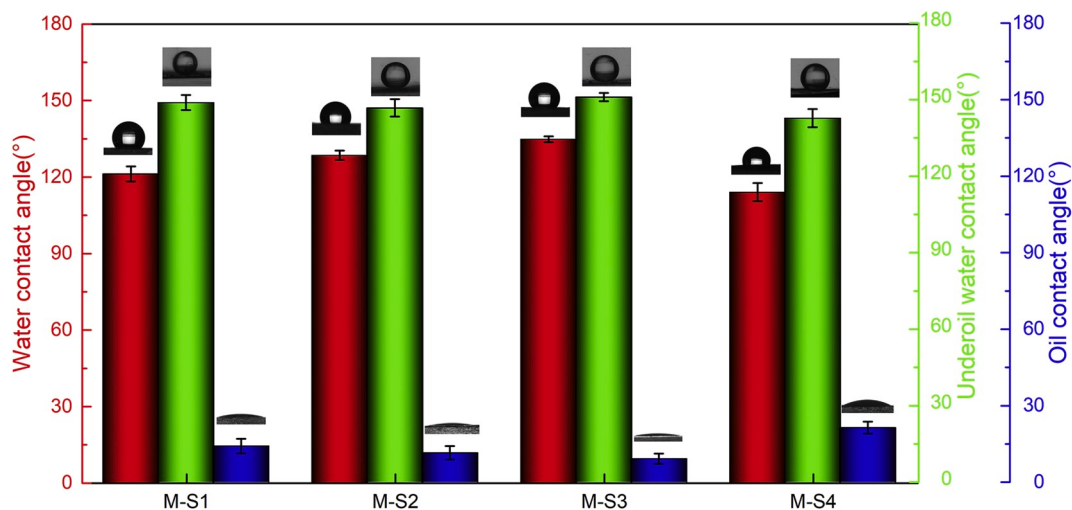


Fig. 10. Images of water contact angle, underoil water contact angle and oil contact angle of NEFS PTFE membrane.

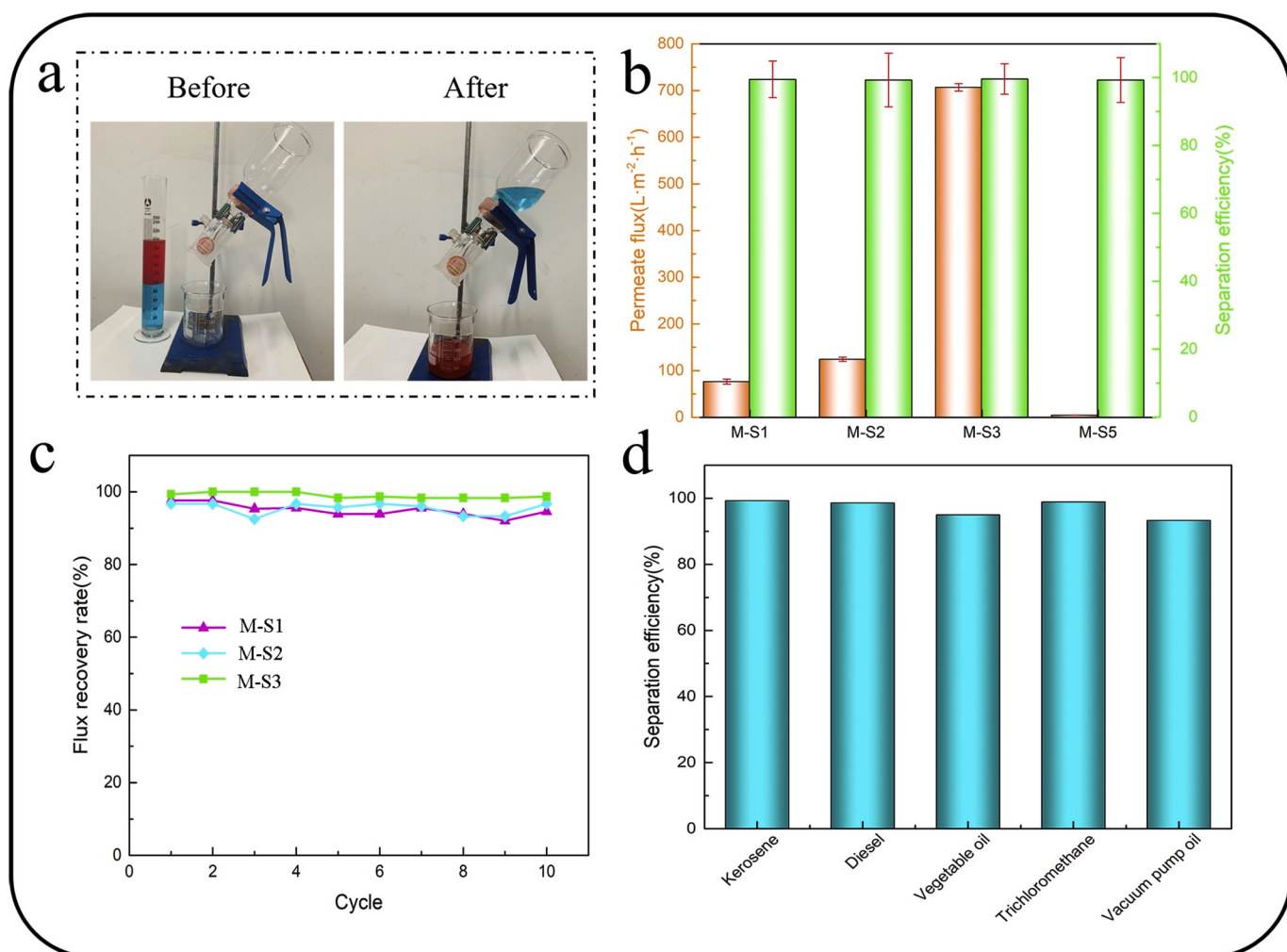


Fig. 11. (a) Images of workflow for oil/water separation; (b) Permeate flux and separation efficiency; (c) Kerosene flux recovery rate after alcohol cleaning; (d) Separation efficiency of different types of oil by M-S3.

PTFE membranes with different pore geometries which was triangular, diamond, square and hexagon, respectively. It can be seen that, the pore shape of obtained NFES PTFE membranes was basically consistent with the CAD design, although there was a little deviation in membrane pore

size between the actual and the CAD design. The pore size of prepared membrane was smaller than the CAD designed owing to the layer of actual membrane which would bring about a smaller pore size. Meanwhile, the movements of PTFE molecular during the sintering process

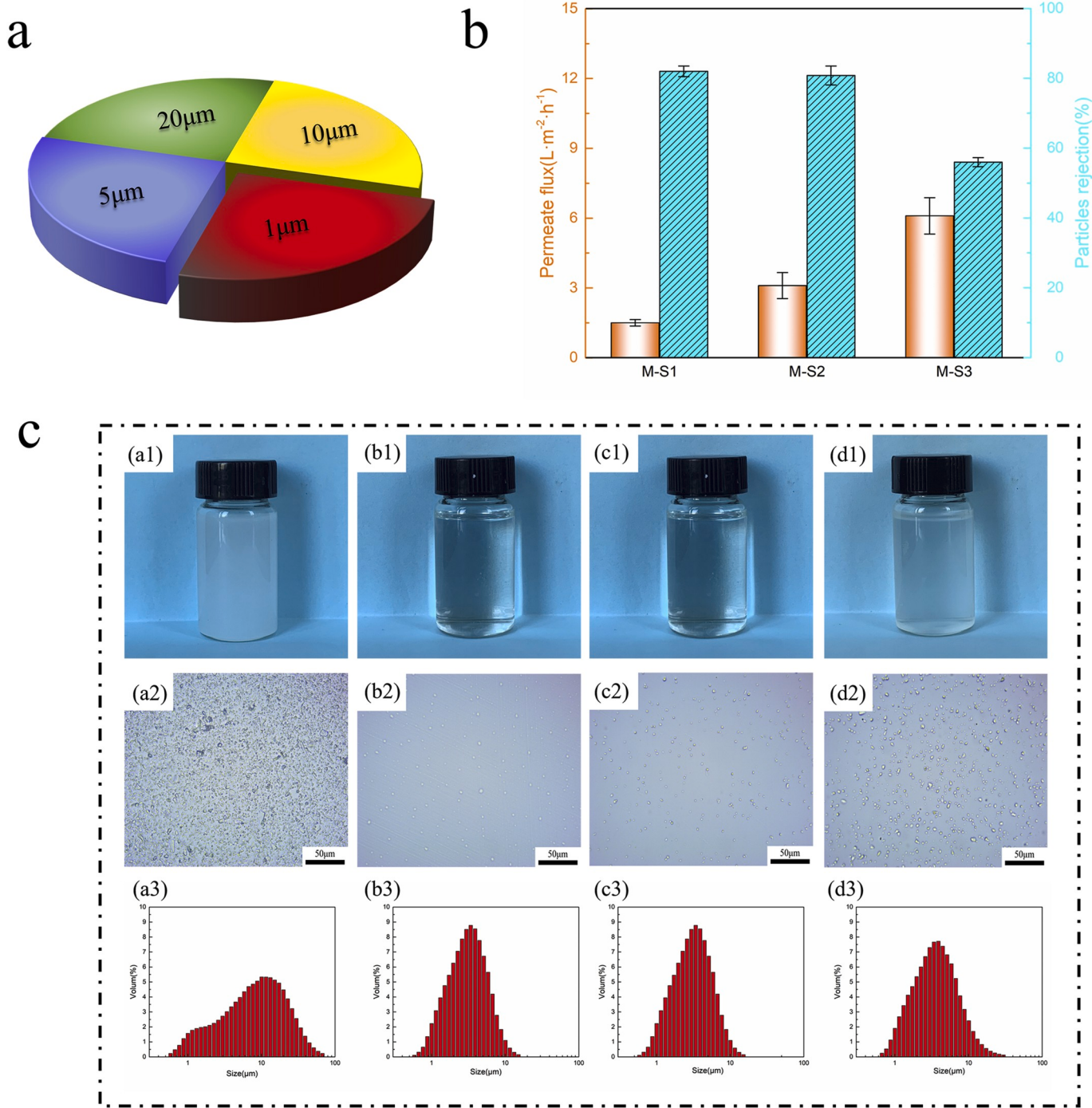


Fig. 12. (a) The pie chart of SiO_2 particle size distribution for sequential filtration experiment; (b) Permeate flux and separation efficiency of sequential filtration experiment; (c) digital images (1), optical microscope images (2), and size distributions images of collected solution (3).

would also induce the fiber edge expansion, which further reduced the pore size.

The images of different pore geometry with the setting side length of 0.2 mm and 6 layers print thickness were shown in Fig. 9. It can be seen that all the membranes showed good pore geometry except M-S4. As for M-S4, it can be seen that there were cracks and pore fusion appeared on the membrane surface. Comparing with other pore geometries, hexagon was easier to confuse during the electrospinning process, which would lead to the stacking of the PTFE particles. That was why the surface of M-S4 had the highest membrane thickness which would induce the temperature imbalance between upper and lower layer, and then further brought out the deflection on membrane surface during the sintering

process.

3.2. Oil/water separation performance

Owing to the excellent hydrophobicity and oleophylicity (Fig. 10), the obtained NFES PTFE membranes were utilized in oil/water separation test. The commercial biaxial stretching PTFE membrane was also used for comparison, which was named M-S5.

Fig. 11a showed the oil/water separation process, it can be seen that the kerosene with red-dye permeated through the NEFS PTFE membrane by self-weight without any extra pressure, which exhibited excellent oil-water separation performance. Fig. 11b showed the results of oil flux

and separation efficiency. It can be seen that M-S3 with square pore geometry showed the highest kerosene flux which was $707 \text{ L m}^{-2} \text{ h}^{-1}$. This was because that the M-S3 membrane with square pore geometry had perforated tunnel structure than the M-S1 with triangle or M-S2 with diamond pore geometry. What's more, the biaxial stretching PTFE membrane M-S5 showed the lowest oil flux because of the node-fibril pore structure which was unfavorable for the oil permeation under the only self-weight pressure. Furthermore, all the three membranes prepared by NFES exhibited excellent oil-water separation efficiency of higher than 99%.

In order to further demonstrate the self-cleaning property of the NFES PTFE membrane, the flux recovery rate was tested (Fig. 11c). It can be found that the all the three membranes' flux recovery rates kept over 95%, which was owing to the low surface energy of PTFE. For further verification, different types of oil were also carried out for oil/water separation, which included kerosene, diesel, trichloromethane, and high viscosity vegetable oil and vacuum pump oil, as shown in Fig. 11d. It was noticeable that the separation efficiencies for various oil/water mixtures reached over 93.3%, which indicated the outstanding oil/water separation performance of NFES PTFE membrane.

3.3. SiO_2 particle sequential separation

Aiming to characterize the regular and accurate pore structure, the NFES PTFE membrane was utilized in the particle sequential separation. The SiO_2 particle sequential separation was tested using with a series of particle sizes ($20 \mu\text{m}$, $10 \mu\text{m}$, $5 \mu\text{m}$ and $1 \mu\text{m}$), which were ultrasonically dispersed in distilled water to form 0.1 wt% feed solution and separated by a cross-flow filtration method. Fig. 12a showed the SiO_2 particle size distributions in the sequential filtration experiments. Fig. 12c was used to verify the separation effect by comparing the feed solution and their collected filtrate. It can be seen that there were plentiful particles of different particle sizes in the feed solution, however, most of $1\text{--}5 \mu\text{m}$ particles were observed after filtrating through M-S1 and M-S2, indicating that the pore size of M-S1 and M-S2 was $5\text{--}10 \mu\text{m}$, while the pore size of M-S3 was $10\text{--}20 \mu\text{m}$. The particle separation experiment not only indirectly proved the membrane pore size from M-S1 to M-S3, but also demonstrated the excellent selective permeability of the NFES PTFE membranes.

4. Conclusions

PTFE membranes with regular geometric pore structure were fabricated by NFES method. Effects of CAD pore geometry, PTFE/PVA mass ratios, sintering temperatures and annealing conditions on the membrane morphology, pore structure and properties were investigated, respectively. The obtained NFES PTFE membrane with square pore structures had excellent oil/water separation efficiency of 99.6% and highest kerosene flux of $707 \text{ L m}^{-2} \text{ h}^{-1}$ under self-weight pressure. Owing to the regular and accurate pore structure, the NFES PTFE membranes could sequential separate SiO_2 particles with a series of particle sizes, with the rejection rate up to 82.0%.

Declaration of competing interest

The authors declare that they have no known competing financial interests or personal relationships that could have appeared to influence the work reported in this paper.

CRediT authorship contribution statement

Jinxue Cheng: Formal analysis, Visualization, Writing - original draft. **Qinglin Huang:** Conceptualization, Investigation, Writing - review & editing. **Yan Huang:** Methodology. **Wei Luo:** Data curation. **Quan Hu:** Software. **Changfa Xiao:** Writing - review & editing.

Acknowledgements

This work was supported by the Science and Technology Plans of Tianjin (No.18PTSYJC00170), the Young Elite Scientists Sponsorship Program by China Association for Science and Technology (No. YESS20160168), and the industrial chain collaborative major projects of the State Oceanic Administration (BHSF2017-01).

References

- [1] M. Padaki, R. Surya Murali, M.S. Abdullah, N. Misran, A. Moslehiani, M.A. Kassim, N. Hilal, A.F. Ismail, Membrane technology enhancement in oil-water separation. a review, *Desalination* 357 (2015) 197–207.
- [2] A. Saxena, B.P. Tripathi, M. Kumar, V.K. Shahi, Membrane-based techniques for the separation and purification of proteins: an overview, *Adv. Colloid Interface Sci.* 145 (2009) 1–22.
- [3] P. Wei, L.-H. Cheng, L. Zhang, X.-H. Xu, H.-l. Chen, C.-j. Gao, A review of membrane technology for bioethanol production, *Renew. Sustain. Energy Rev.* 30 (2014) 388–400.
- [4] J. Cui, A. Xie, S. Zhou, S. Liu, Q. Wang, Y. Wu, M. Meng, J. Lang, Z. Zhou, Y. Yan, Development of composite membranes with irregular rod-like structure via atom transfer radical polymerization for efficient oil-water emulsion separation, *J. Colloid Interface Sci.* 533 (2019) 278–286.
- [5] K. Chen, C. Xiao, H. Liu, G. Li, X. Meng, Structure design on reinforced cellulose triacetate composite membrane for reverse osmosis desalination process, *Desalination* 441 (2018) 35–43.
- [6] D. Eumine Suk, T. Matsuuwa, Membrane-Based hybrid processes: a review, *Separ. Sci. Technol.* 41 (2006) 595–626.
- [7] J. Yong, Y. Fang, F. Chen, J. Huo, Q. Yang, H. Bian, G. Du, X. Hou, Femtosecond laser ablated durable superhydrophobic PTFE films with micro-through-holes for oil/water separation: separating oil from water and corrosive solutions, *Appl. Surf. Sci.* 389 (2016) 1148–1155.
- [8] W. Qing, X. Shi, Y. Deng, W. Zhang, J. Wang, C.Y. Tang, Robust superhydrophobic-supercapophilic polytetrafluoroethylene nanofibrous membrane for oil/water separation, *J. Membr. Sci.* 540 (2017) 354–361.
- [9] A. Ranjbarzadeh-Dibazar, P. Shokrollahi, J. Barzin, A. Rahimi, Lubricant facilitated thermo-mechanical stretching of PTFE and morphology of the resulting membranes, *J. Membr. Sci.* 470 (2014) 458–469.
- [10] C. Su, Y. Li, H. Cao, C. Lu, Y. Li, J. Chang, F. Duan, Novel PTFE hollow fiber membrane fabricated by emulsion electrospinning and sintering for membrane distillation, *J. Membr. Sci.* 583 (2019) 200–208.
- [11] J.-Y. Park, J.-H. Lee, C.-H. Kim, Y.-J. Kim, Fabrication of polytetrafluoroethylene nanofibrous membranes for guided bone regeneration, *RSC Adv.* 8 (2018) 34359–34369.
- [12] R.D. Gustafson, A.L. McGaughey, W. Ding, S.C. McVety, A.E. Childress, Morphological changes and creep recovery behavior of expanded polytetrafluoroethylene (ePTFE) membranes used for membrane distillation, *J. Membr. Sci.* 584 (2019) 236–245.
- [13] D.L. Kerbow, C.A. Sperati, *Physical Constants of Fluoropolymers*, 2003.
- [14] X. Li, X.X. Wang, T.T. Yue, Y. Xu, M.L. Zhao, M. Yu, S. Ramakrishna, Y.Z. Long, Waterproof-breathable PTFE nano- and microfiber membrane as high efficiency PM2.5 filter, *Polymers* (2019) 11.
- [15] Q.-L. Huang, C.-f. Xiao, X.-y. Hu, A novel method to prepare hydrophobic poly(tetrafluoroethylene) membrane, and its properties, *J. Mater. Sci.* 45 (2010) 6599–6573.
- [16] H. Zhu, H. Wang, F. Wang, Y. Guo, H. Zhang, J. Chen, Preparation and properties of PTFE hollow fiber membranes for desalination through vacuum membrane distillation, *J. Membr. Sci.* 446 (2013) 145–153.
- [17] D. Vavlekas, M. Ansari, H. Hao, F. Fremy, J.L. McCoy, S.G. Hatzikiriakos, Zero Poisson's ratio PTFE in uniaxial extension, *Polym. Test.* 55 (2016) 143–151.
- [18] C. Chang, K. Limkrailassiri, L. Lin, Continuous near-field electrospinning for large area deposition of orderly nanofiber patterns, *Appl. Phys. Lett.* 93 (2008) 123111.
- [19] X.-X. He, J. Zheng, G.-F. Yu, M.-H. You, M. Yu, X. Ning, Y.-Z. Long, Near-field electrospinning: progress and applications, *J. Phys. Chem. C* 121 (2017) 8663–8678.
- [20] R. Middleton, X. Li, J. Shepherd, Z. Li, W. Wang, S.M. Best, R.E. Cameron, Y.Y. S. Huang, Near-field electrospinning patterning polycaprolactone and polycaprolactone/collagen interconnected fiber membrane, *Macromol. Mater. Eng.* 303 (2018) 1700463.
- [21] G.S. Bisht, G. Canton, A. Mirsepassi, L. Kulinsky, S. Oh, D. Dunn-Rankin, M. J. Madou, Controlled continuous patterning of polymeric nanofibers on three-dimensional substrates using low-voltage near-field electrospinning, *Nano Lett.* 11 (2011) 1831–1837.
- [22] Q. Huang, Y. Huang, S. Gao, M. Zhang, C. Xiao, Novel ultrafine fibrous poly(tetrafluoroethylene) hollow fiber membrane fabricated by electrospinning, *Polymers* (2018) 10.
- [23] M. Conte, B. Pinedo, A. Igartua, Role of crystallinity on wear behavior of PTFE composites, *Wear* 307 (2013) 81–86.
- [24] Q.-L. Huang, C.-f. Xiao, X.-s. Feng, X.-Y. Hu, Design of super-hydrophobic microporous polytetrafluoroethylene membranes, *New J. Chem.* 37 (2013) 373–379.